


**Genesis and atomic structure of the charge density wave phase of 1T-VSe<sub>2</sub>**V. Petkov<sup>1,\*</sup>, A. Zafar,<sup>1</sup> M. Jakhar,<sup>1</sup> and AM Milinda Abeykoon<sup>2</sup><sup>1</sup>*Department of Physics, Central Michigan University, Mt. Pleasant, Michigan 48858, USA*<sup>2</sup>*Photon Sciences Division, Brookhaven National Laboratory, Upton, New York 11973, USA* (Received 21 September 2024; revised 10 December 2024; accepted 12 December 2024; published 15 January 2025)

Using variable temperature total x-ray scattering, we study the emergence of charge density wave (CDW) order in the archetypal transition-metal dichalcogenide (TMDC) 1T-VSe<sub>2</sub>. We find that a CDW precursor phase (PF) appears at  $T_{\text{CDW(PF)}}$  of 200(5) K, where V and Se atoms experience in- and out-of-plane static displacements from their position in the undistorted lattice, respectively. The displacements increase with decreasing temperature and a little-known superstructure of V triatomic clusters emerges below  $T_{\text{CDW(3D)}}$  of 100(5) K, where three-dimensional CDW order sets in. Concurrently, Se atoms form less well-defined dimers. Thus, similarly to other TMDCs, 1T-VSe<sub>2</sub> appears to exhibit a two-step CDW transition. The finding underlines the key contribution of lattice distortions to the emergence of CDW order in 1T-VSe<sub>2</sub> and generally in TMDCs.

DOI: [10.1103/PhysRevB.111.014105](https://doi.org/10.1103/PhysRevB.111.014105)**I. INTRODUCTION**

Because of strong correlations between its electronic, lattice, charge, and spin degrees of freedom, the archetypal transition-metal dichalcogenide (TMDC) 1T-VSe<sub>2</sub> hosts a rich variety of unusual physical phenomena, such as charge density waves (CDWs), metal-insulator transitions, pressure-induced superconductivity, Weyl semimetal, and spin liquid states [1–16]. However, despite decades of research, their origin remains not well understood. This is especially true for the CDW order that is considered to arise either from Fermi surface nesting [17–19] or strong electron-phonon coupling effects [20–25]. The controversy has been addressed in recent comprehensive studies [26–30], but the lack of a universal agreement on the origin of CDWs in TMDCs in general and in 1T-VSe<sub>2</sub> in particular remains.

Among other octahedral 1T-TMDCs exhibiting CDW phenomena such as 1T-TiSe<sub>2</sub> ( $T_{\text{CDW}} = 200$  K) and 1T-TaSe<sub>2</sub> ( $T_{\text{CDW}} = 473$  K), 1T-VSe<sub>2</sub> is unique because it develops anomalies in its transport and magnetic properties that more closely resemble those observed with trigonal prismatic 2H-TMDCs such as 2H-NbSe<sub>2</sub> ( $T_{\text{CDW}} = 33$  K) and 2H-TaSe<sub>2</sub> ( $T_{\text{CDW}} = 122$  K) [31–38], where  $T_{\text{CDW}}$  is the respective CDW transition temperature. It has a layered structure with a trigonal space group (SG)  $P\bar{3}m1$  symmetry, where each layer features a hexagonal plane of V atom sandwiched between two hexagonal planes of Se atoms [39]. In a layer, V and Se atoms form distorted octahedra, as shown in Fig. 1(a). Diffraction studies have suggested that, upon cooling, 1T-VSe<sub>2</sub> exhibits a variety of superstructure formations, including an incommensurate superstructure appearing in the 110–140 K range and a three-dimensional (3D) commensurate  $4a \times 4a \times 3c$  superstructure setting in below  $T_{\text{CDW(3D)}} = 100$  K, where  $a$  and  $c$  are the parameters of the undistorted lattice [40–43].

Concurrent changes in the electronic structure have been observed, including a partial suppression of the density of states (DOS) below 180 K. It has been shown that the emerged pseudogap is in the order of 40–60 meV and opens over small portions of the Fermi surface, which is consistent with the fact that the electrical resistivity of 1T-VSe<sub>2</sub> remains metallic in character below  $T_{\text{CDW(3D)}}$  [1,44–49]. The changes in the crystal and electronic structure have been associated with the presence of a soft-phonon mode with a propagation vector close to  $q_{\text{CDW}}(1/4,0,1/3)$  [26,29,50]. Single-crystal diffuse scattering has indeed found evidence for the presence of a mixture of longitudinal and transverse phonons at temperatures below 200 K [26,30,51], but the temperature evolution of the atomic displacement modes has never been studied in detail. Here we reveal it by total x-ray scattering experiments coupled to atomic pair distribution function (PDF) analysis, which has proven very useful in structural studies of materials exhibiting lattice distortions, including CDW phases of TMDCs [38,52,53]. We find that the CDW order emerges from a CDW precursor phase (PF) that exists between  $T_{\text{CDW(PF)}} = 200(5)$  K and  $T_{\text{CDW(3D)}} = 100(5)$  K, below which a  $4a \times 4a \times 3c$  superstructure sets in. In the superstructure, V atoms form clusters resembling equilateral triangles while Se atoms form less well-defined dimers. Our study resolves the so far unknown atomic ordering pattern in CDW 1T-VSe<sub>2</sub> and shows that lattice distortions emerge well above  $T_{\text{CDW(3D)}}$ , i.e., are intrinsic to the material, underlining their key contribution to the CDW phenomena it exhibits.

**II. EXPERIMENT**

We studied a high-quality sample provided by 2D Semiconductors [54]. To illustrate the effect of the CDW transition on the electronic properties, we measured the temperature evolution of the magnetic susceptibility [Fig. 1(b)]. In line with results from prior studies [29,55], the susceptibility is seen to decrease near linearly with

\*Contact author: petko1vg@cmich.edu

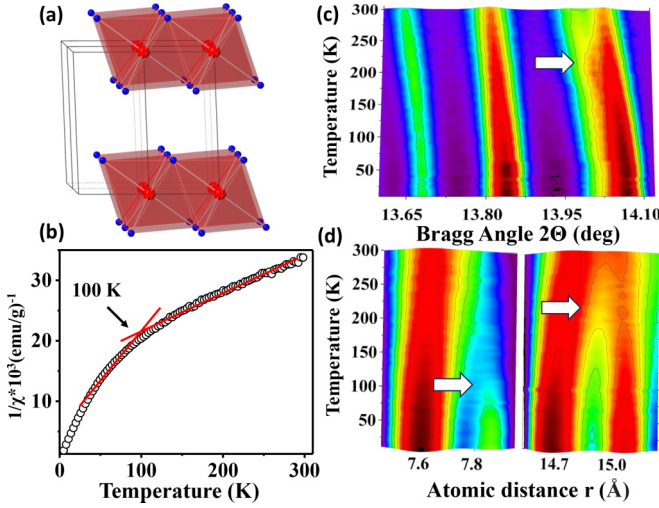


FIG. 1. (a) Unit cell for undistorted 1T-VSe<sub>2</sub> (thin line) with V centered octahedra (red) shown. (b) Temperature evolution of the magnetic susceptibility for 1T-VSe<sub>2</sub> indicating the presence of a broad phase transition at about  $T_{\text{CDW}(3\text{D})} = 100(5)$  K. Intensity color maps of selected peaks in experimental (c) XRD patterns and (d) atomic PDFs. Arrows mark intensity changes taking place at about  $T_{\text{CDW}(3\text{D})} = 100(5)$  K and  $T_{\text{CDW}(PF)} = 200(5)$  K. Red lines in (b) are a guide to the eye.

temperature down to about 100(5) K, where the decrease accelerates. The observed nonlinearity is attributed to a reduction of DOS at the Fermi level occurring when 3D CDW order sets in.

Synchrotron x-ray diffraction (XRD) experiments were performed at the beamline 28-ID-1 at the National Synchrotron Source-II, Brookhaven National Laboratory, using x-rays with energy of 74.46 keV ( $\lambda = 0.1665$  Å). The powder sample packed in a Kapton tube was kept inside a liquid He cryostat used to control its temperature. Scattered x-ray intensities were collected with a PerkinElmer area detector while decreasing the temperature from 300 to 10 K in steps of 5 K. Atomic PDFs were derived from the experimental XRD patterns using standard procedures [56,57]. Intensity color maps of the patterns and respective PDFs are shown in Figs. 1(c) and 1(d), respectively. Intensity variations are clearly seen at temperatures close to 200(5) K and  $T_{\text{CDW}(3\text{D})} = 100(5)$  K, indicating the presence of significant changes in the crystal structure. The concurrent nonlinearity in the temperature dependencies of the magnetic susceptibility and PDF peak intensities indicates the presence of a strong interaction between the electronic and lattice degrees of freedom in 1T-VSe<sub>2</sub>.

### III. STRUCTURE MODELING

To assess the average crystal structure of 1T-VSe<sub>2</sub>, the experimental XRD patterns were subjected to Rietveld analysis [58] based on a trigonal SG  $P\bar{3}m1$  structure model. Representative Rietveld fits to patterns obtained at 300, 150, and 20 K are shown in Figs. 2(a)–2(c). The model reproduces the XRD data well, confirming the phase purity of our sample and lack of texture effects. Refined values for the  $a$  and  $c$  lattice parameters and unit cell volume are shown in Figs. 2(d) and 2(e). Their temperature evolution shows a nonlinearity in the

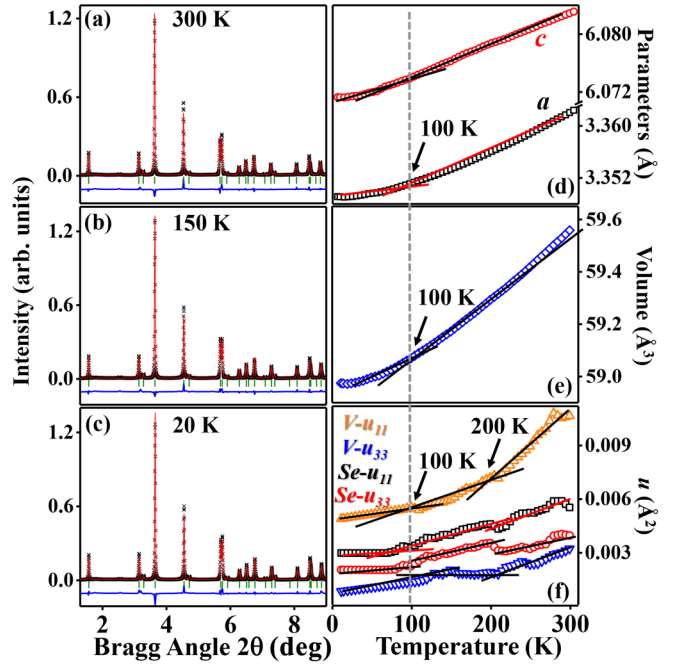


FIG. 2. (a)–(c) Rietveld fits (red) to selected XRD patterns (symbols) for 1T-VSe<sub>2</sub> based on an undistorted SG  $P\bar{3}m1$  type structure. The residual difference (blue) is shifted for clarity. The goodness-of-fit indicator is about 9 % for all fits. (d)–(f) Temperature evolution of Rietveld refined (d) lattice parameters, (e) unit cell volume, and (f) in-plane ( $u_{11}$ ) and out-of-plane ( $u_{33}$ ) thermal factors for V and Se atoms. Arrows point to inflection points in the respective curves that appear close to  $T_{\text{CDW}(3\text{D})} = 100(5)$  K and  $T_{\text{CDW}(PF)} = 200(5)$  K. Black and red lines in (d)–(f) are a guide to the eye.

vicinity of  $T_{\text{CDW}(3\text{D})}$ . In line with results from prior studies [1,26,30,59,60], our density functional theory (DFT) calculations based on Rietveld refined structure data showed that the charge carriers at the Fermi level come mostly from V bands (see Fig. S1 in the Supplemental Material [61]) and the crystal lattice exhibits a soft-phonon mode type instability (Fig. S2) at a wave vector close to  $q_{\text{CDW}}(1/4,0,1/3)$ . Refined values for the in- ( $u_{11}$ ) and out-of-plane ( $u_{33}$ ) thermal factors for V and Se atoms, which reflect both trivial thermal and eventual static atomic displacements, are shown in Fig. 2(f). The  $u_{11}$  for V atoms appears much larger than the other thermal factors shown in Fig 2(f), suggesting the presence of a considerable atomic positional disorder in the V planes. The temperature evolution of  $u_{33}$  for V and that of  $u_{11}$  and  $u_{33}$  for Se atoms is, however, not well expressed because, generally, Rietveld analysis has a limited sensitivity to weak lattice distortions.

To investigate the atomic positional disorder in more detail, we approached the experimental atomic PDFs with the same structure model using the software PDFGUI [65]. Representative PDF fits to PDF data obtained at 300, 150, and 20 K are shown in Figs. 3(a)–3(c) and 4(a)–4(c). The SG  $P\bar{3}m1$  structure model reproduced very well the experimental data for undistorted 1T-VSe<sub>2</sub> obtained at 300 K. However, it failed to reproduce well the 150 and 20 K PDF data sets. Models found useful in describing the CDW phases of sister compounds of 1T-VSe<sub>2</sub>, such as 1T-TiSe<sub>2</sub> and 1T-TaSe<sub>2</sub> [66,67], performed much worse when attempting to fit the

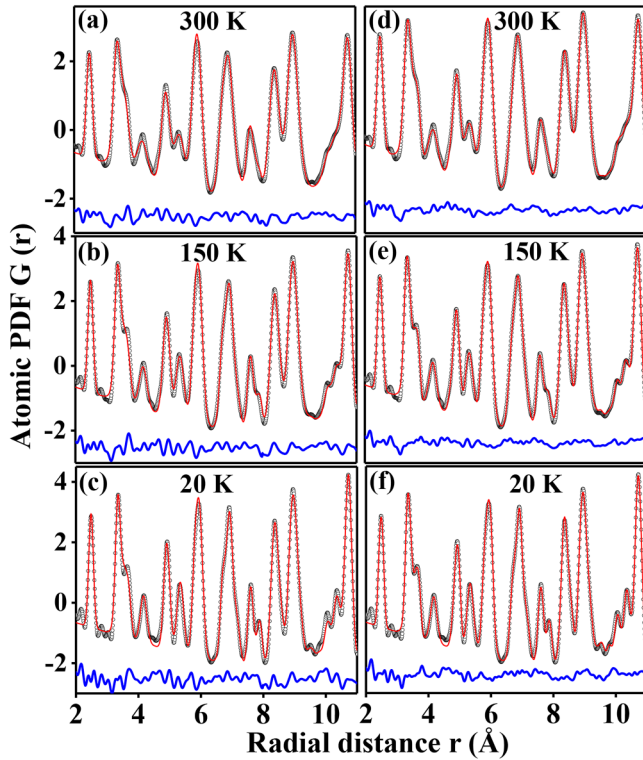


FIG. 3. Fits (red) to selected atomic PDFs (symbols) for  $17\text{-VSe}_2$ . The residual difference (blue) is shifted for clarity. The fits in (a)–(c) are based on an undistorted SG  $P\bar{3}m1$ -type structure. The goodness-of-fit factor for the fits varies from 10% for the 300-K data set to 16% for the 20-K data set. The fits in (d)–(f) are based on a  $4a \times 4a \times 3c$  superstructure described in the text. The goodness-of-fit factor for the fits is about 9%.

150 and 20 K PDF data sets (see Fig. 5). On the other hand, a model featuring a  $4a \times 4a \times 3c$  superstructure derived from the undistorted SG  $P\bar{3}m1$ -type structure performed very well, as the data in Figs. 3(d)–3(f) and 4(d)–4(f) show. Note that, contrary to the case of the undistorted model, V atoms in the  $4a \times 4a \times 3c$  superstructure model are allowed to change their positions such that the agreement between model computed and experimental PDF data is improved. Refined positions for V and Se atoms in  $17\text{-VSe}_2$  at 20 and 150 K are given as Supplemental Material [61]. Refined values for the  $a$  and  $c$  lattice parameters and unit cell volume are summarized in Figs. 6(a) and 6(b). Their temperature evolution shows clear discontinuities at 200(5) K and  $T_{\text{CDW}(3\text{D})} = 100(5)$  K, indicating the presence of two distinct steps in the temperature evolution of the crystal structure of  $17\text{-VSe}_2$ . The temperature evolution of the in- and out-of-plane static displacements of V and Se from their high-temperature equilibrium positions in the undistorted lattice [Figs. 6(c) and 6(d)] also shows clear discontinuities at 200(5) K and  $T_{\text{CDW}(3\text{D})} = 100(5)$  K.

#### IV. DISCUSSION

In the  $4a \times 4a \times 3c$  superstructure, there are two sets of inequivalent V planes, V(1) and V(2), and three sets of inequivalent Se planes, Se(1)–Se(3), as shown in Fig. S3 [61].

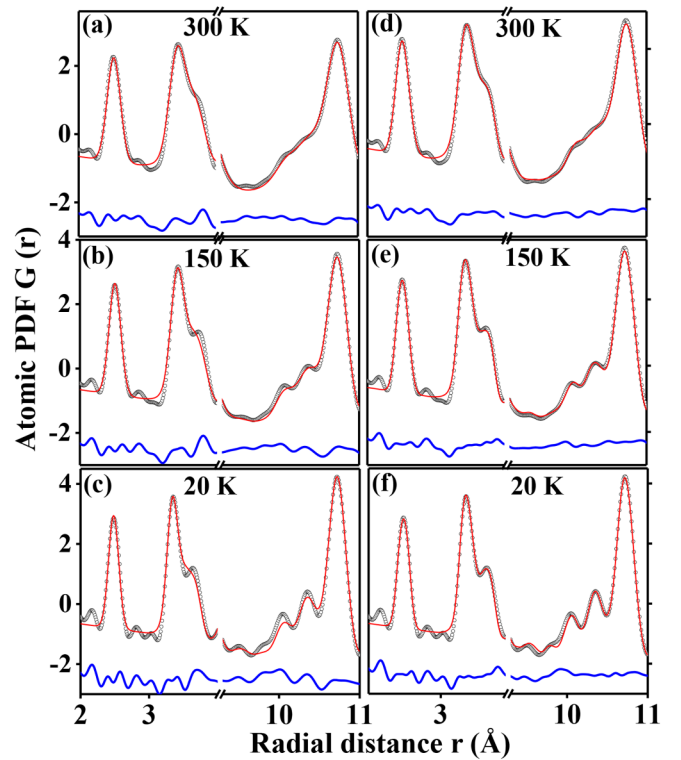


FIG. 4. Segments from the PDF fits (red) shown in Fig. 3 elucidating their performance. The residual difference (blue) is shifted for clarity. The fits in (a)–(c) are based on an undistorted SG  $P\bar{3}m1$ -type structure. The fits in (d)–(f) are based on a  $4a \times 4a \times 3c$  superstructure described in the text. The superstructure fit does not greatly outperform the undistorted structure fit to the 300 K PDF data. However, it is clearly superior to the undistorted structure fits to the 20- and 150-K PDF data [(e),(f)] in reproducing fine PDF features, including the higher- $r$  component of the PDF peak at 3.5 Å and the series of low-intensity PDF peaks positioned between 9.5 and 10.5 Å.

Results of the PDF fits show that atoms in both V(1) and V(2) planes exhibit only in-plane displacements with decreasing temperature [Fig. 6(c)]. In particular, the displacements in the V(1) planes already appear at room temperature and sharply increase at 200(5) K. The increase accelerates further at  $T_{\text{CDW}(3\text{D})} = 100(5)$  K. In the V(2) planes, the displacements appear at 200(5) K and gradually increase with decreasing temperature. On the other hand, atoms in the Se(1)–Se(3) planes hardly exhibit in-plane displacements down to 10 K. However, they exhibit considerable out-of-plane displacements that increase gradually below 200(5) K and remain nearly constant below  $T_{\text{CDW}(3\text{D})}$  [see Figs. 6(c) and 6(d)]. The arrangement of atoms in the V and Se planes at 300 and 20 K is shown in Figs. 7(a)–7(d). That at 150 K, which is characteristic to the precursor phase, is shown in Fig. S4 [61]. At 300 K, i.e., in undistorted  $17\text{-VSe}_2$ , both V and Se atoms form perfect hexagons where all V-V and Se-Se distances are about 3.36 Å. At 150 K, V and Se atoms form somewhat distorted hexagons, where some V-V and Se-Se distances differ from the average bond length distance of 3.35 Å, but the difference is less than 1%. At 20 K, i.e., in the CDW phase, several V and Se atoms experience large static displacements, leading to the

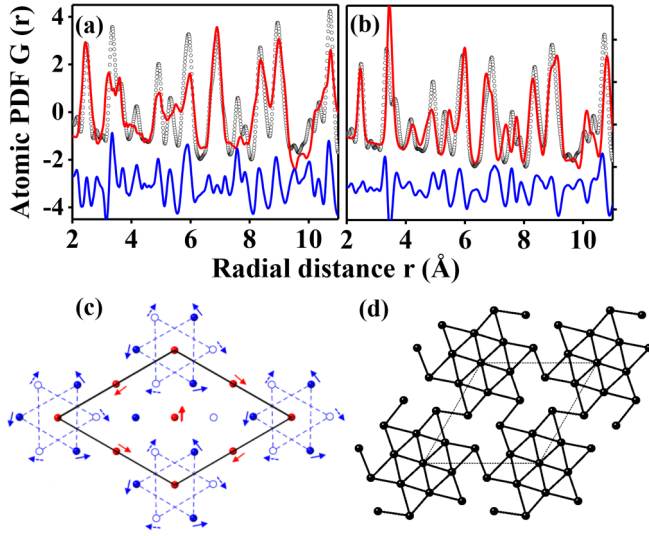


FIG. 5. Unsuccessful fits (red line) to PDF data (symbols) for  $1T$ -VSe<sub>2</sub> obtained at 20 K. The residual difference (blue) is shifted for clarity. The fit in (a) is based on a  $2a \times 2a \times 2c$  CDW superstructure (c) found useful in describing the CDW phase of  $1T$ -TiSe<sub>2</sub> [63]. The fit in (b) is based on a  $\sqrt{13}a \times \sqrt{13}a \times 13c$  CDW superstructure (d) found useful in describing the CDW phase of  $1T$ -TaSe<sub>2</sub> [64]. Red and blue circles in (c) represent Ti and Se atoms, respectively, while arrows show their displacement during the CDW phase transitions. The unit cell is outlined with a thick black line. Black circles in (d) represent Ta atoms forming star-of-David-like clusters. The unit cell is outlined with a broken blue line.

emergence of a variety of V-V and Se-Se distances that range from 3.06 to 3.50 Å and from 3.26 to 3.38 Å, respectively. In particular, a V-V distance of 3.06 Å between atoms forming clusters resembling equilateral triangles appears in the V(1) planes [Fig. 7(e)]. The displacements of atoms in the V(2) planes are smaller in magnitude, yet a large number of V-V distances that are shorter or longer than the average one (3.34 Å) by more than 1% exist [Fig. 7(c)]. Concurrently, a large number of Se-Se distances in the Se(1)–Se(3) planes appear shorter (3.26 Å) or longer (3.38 Å) than the average bond length distance by more than 1%. The shorter distance is between atoms forming dimers [Figs. 7(g)–7(i)]. Overall, the atomic displacements in V and those in the Se planes differ both in direction and magnitude, leading to the formation of different configurations of atoms that do not sit on the vertices of regular hexagons. Notably, the atomic configurations in the V planes are of the type discussed in the early studies of the CDW order in  $1T$ -VSe<sub>2</sub> [41].

The picture that emerges is the following. Upon decreasing temperature below 300 K, atoms in the V(1) planes increasingly experience in-plane atomic displacements that rise sharply at 200(5) K and keep increasing nonlinearly with further cooling of the sample, exhibiting a kink at  $T_{\text{CDW}(3\text{D})}$ . By contrast, Se atoms hardly experience in-plane displacements down to 20 K while their out-of-plane displacements start increasing below 200(5) K. Evidently, the CDW phase transition in  $1T$ -VSe<sub>2</sub> is a two-step process that includes a precursor phase (PF) existing over a wide temperature range from  $T_{\text{CDW}(PF)} = 200(5)$  K to  $T_{\text{CDW}(3\text{D})} = 100(5)$  K. In the

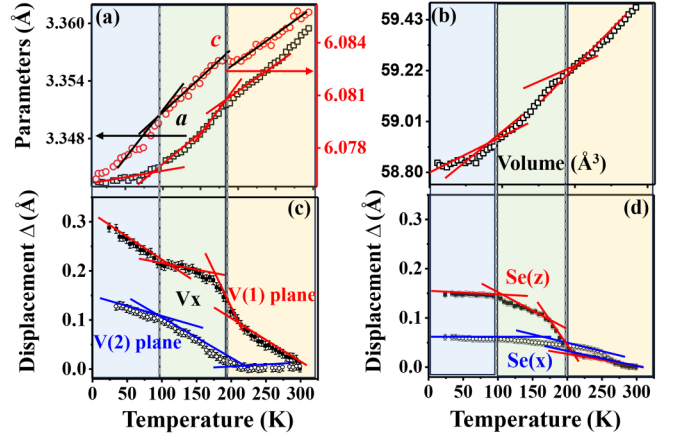


FIG. 6. [(a),(b)] Temperature evolution of the PDF refined lattice parameters  $a$  and  $c$  and unit cell volume for  $1T$ -VSe<sub>2</sub> based on a  $4a \times 4a \times 3c$  superstructure model. (c) Temperature evolution of the in-plane ( $V_x$ ) static displacements,  $\Delta$ , for atoms from the V(1) and V(2) planes (see Fig. S1) in the superstructure. (d) Typical temperature evolution of the in-plane Se(x) and out-of-plane Se(z) static displacements,  $\Delta$ , for Se atoms in the superstructure. All data sets exhibit inflection points at  $T_{\text{CDW}(3\text{D})} = 100(5)$  K and  $T_{\text{CDW}(PF)} = 200(5)$  K. Black, blue, and red lines in (a)–(d) are a guide to the eye. Vertical broken lines separate temperature regions where the material appears in its undistorted (light brown), CDW precursor (light green), and 3D CDW (light blue) phase.

phase, V atoms are displaced from their average in-plane positions while, largely, Se atoms are displaced from their average out-of-plane positions, leading to a disruption of the hexagonal atomic ordering pattern (see Fig. S4) characteristic to room temperature  $1T$ -VSe<sub>2</sub>. Upon further cooling the material, the displacements of V and Se atoms both increase in magnitude and couple over long-range distances, leading to the emergence of a  $4a \times 4a \times 3c$  superstructure below  $T_{\text{CDW}(3\text{D})}$  that features V trimers and Se dimers. The presence of a precursor phase may well explain the emergence of a “precursor” CDW pseudogap well above  $T_{\text{CDW}(3\text{D})}$  and its smooth evolution with decreasing temperature [1,43–48]. Notably,  $1T$ -VSe<sub>2</sub> monolayers (MLs) have been shown to exhibit CDW order at a temperature of about 220 K [68–70], which is close to  $T_{\text{CDW}(PF)}$ . Evidently, the material can be added to the list of octahedral  $1T$ -TMDCs where the CDW order appears enhanced in the ML limit in comparison to the bulk phase such as, for example,  $1T$ -NbSe<sub>2</sub> ( $T_{\text{CDW}(3\text{D})} = 33$  K vs  $T_{\text{CDW}(ML)} = 145$  K) and  $1T$ -TiSe<sub>2</sub> ( $T_{\text{CDW}(3\text{D})} = 205$  K vs  $T_{\text{CDW}(ML)} = 235$  K). A similar effect is also observed with trigonal prismatic  $2H$ -TMDCs such as  $2H$ -TaSe<sub>2</sub> and  $2H$ -NbSe<sub>2</sub> [38,71–73]. In all these systems, due to weak interlayer coupling, 2D lattice distortions related to CDW order emerge before charge modulations become 3D ordered over long-range distances.

## V. CONCLUSION

Among other octahedral  $1T$ -TMDCs,  $1T$ -VSe<sub>2</sub> exhibits a unique CDW superstructure involving di- and triatomic clusters. Signatures of the superstructure emerge at 200(K)

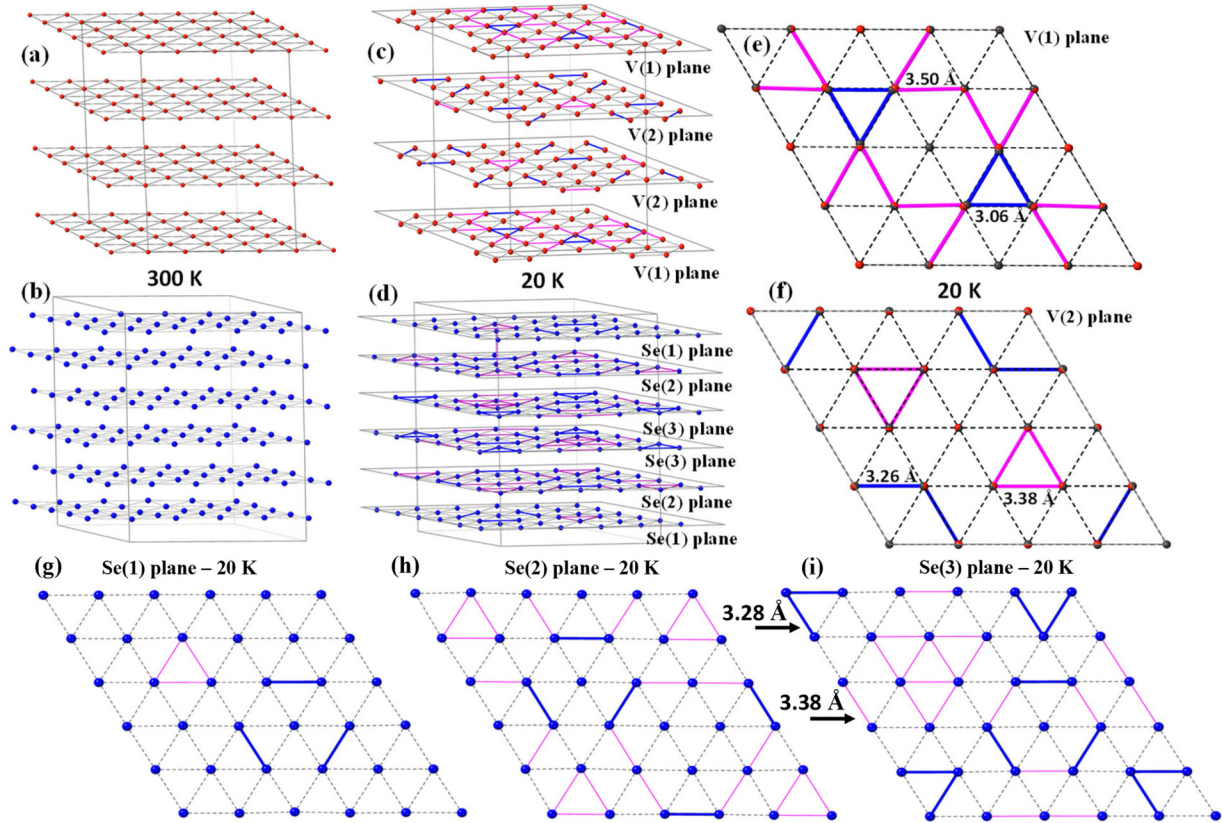


FIG. 7. [(a), (b)] Vanadium (red) and Se (blue) atomic planes in undistorted  $1T\text{-VSe}_2$  at 300 K. In the planes, all V-V and Se-Se distances (thin black line) are  $3.36 \text{ \AA}$  in length. [(c), (d)] Vanadium (red) and Se (blue) atomic planes in CDW  $1T\text{-VSe}_2$  at 20 K. In the planes, there exist V-V and Se-Se distances that are at least 1% longer (magenta) or shorter (blue) than the average bonding distances (thin black line) of  $3.34 \text{ \AA}$ . Projection of (e) V(1) and (f) V(2) planes down the  $c$  axis of the crystal lattice. In the V(1) planes, atoms are seen to assemble in equilateral triangles (thick blue lines) while less well-defined dimers (thick blue lines) appear in the V(2) planes. (g)–(i) Projection of (g) Se(1), (h) Se(2), and (i) Se(3) planes down the  $c$  axis of the crystal lattice in CDW  $1T\text{-VSe}_2$ . In the CDW phase, Se atoms appear displaced from their average positions, leading to the formation of dimers of Se atoms (blue lines) positioned considerably closer ( $3.28 \text{ \AA}$ ) in comparison to the average Se-Se ( $3.34 \text{ \AA}$ ) distance. Magenta lines in (e)–(i) represent interatomic distances that are longer than the average bond length of  $3.34 \text{ \AA}$ .

as a CDW precursor phase via a well-defined phase transition. The complete 3D CDW superstructure sets in when the temperature is further reduced below  $100(5) \text{ K}$ . The electronic properties appear to track the unusual structural evolution. Thus, our results not only shed light on the genesis of CDWs in  $1T\text{-VSe}_2$  but also highlight the key contribution of lattice distortions to CDW phenomena in TMDCs.

## ACKNOWLEDGMENTS

Thanks are due to Dr. R. Amin for preliminary analysis of the experimental data. This work was supported by the U.S. Department of Energy, Office of Science, Office of Basic Energy Sciences under Award No. DE-SC0021973 and used resources of the National Synchrotron Light Source at the Brookhaven National Laboratory provided by the DOE Office of Science under Contract No. DE-SC0012704.

- [1] W. Jolie, T. Knispel, N. Ehlen, K. Nikonov, C. Busse, A. Gruneis, and T. Michely, Charge density wave phase of  $\text{VSe}_2$  revisited, *Phys. Rev. B* **99**, 115417 (2019).
- [2] S. Sahoo, U. Dutta, L. U. Harnagea, A. K. Sood, and S. Karmakar, Pressure-induced suppression of charge density wave and emergence of superconductivity in  $1T\text{-VSe}_2$ , *Phys. Rev. B* **101**, 014514 (2020).
- [3] K. Xu, P. Chen, X. Li, C. Wu, Y. Guo, J. Zhao, X. Wu, and Y. Xie, Ultrathin nanosheets of vanadium diselenide: A metallic two-dimensional material with ferromagnetic charge-density-wave behavior, *Angew. Chem.* **125**, 10671 (2013).
- [4] D. J. Eaglesham, R. L. Withers, and D. M. Bird, Charge-density-wave transitions in  $1T\text{-VSe}_2$ , *J. Phys. C: Solid State Phys.* **19**, 359 (1986).
- [5] S. Mohanty and P. Deb, Nontrivial band topology coupled thermoelectrics in  $\text{VSe}/\text{MoSe}_2$  van der Waals magnetic Weyl semimetal, *J. Phys.: Condens. Matter.* **34**, 335801 (2022).
- [6] D. Biswas *et al.*, Ultrafast triggering of insulator–metal transition in two-dimensional  $\text{VSe}_2$ , *Nano Lett.* **21**, 1968 (2021).
- [7] M. A. Jafari, M. Wawrzyniak-Adamczewska, S. Stagraczyński, A. Dyrdał, and J. Barnaś, Spin valve effect in two-dimensional  $\text{VSe}_2$  system, *J. Magn. Magn. Mater.* **548**, 168921 (2022).

- [8] H. Li, G. He, Y. Qin, J. Yang, and Y. Peng, Stochastic resonance of two coupled fractional harmonic oscillators in Jerk equation, *Results Phys.* **50**, 106533 (2023).
- [9] G. Grüner, The dynamics of charge-density waves, *Rev. Mod. Phys.* **60**, 1129 (1988).
- [10] S. Barua, M. C. Hatnean, M. R. Lees, and G. Balakrishnan, Signatures of the Kondo effect in  $VSe_2$ , *Sci. Rep.* **7**, 10964 (2017).
- [11] Q. Jiang, W. Xia, T. Xu, W. Liu, X. Shen, Y. Guo, M. Ye, and S. Qiao, Independent spin polarized valence electronic states in  $VSe_2$  from charge density wave transition, *J. Electron Spectros. Relat. Phenom.* **238**, 146868 (2020).
- [12] W. Liao, S. Zhao, F. Li, C. Wang, Y. Ge, H. Wang, S. Wang, and H. Zhang, Interface engineering of two-dimensional transition metal dichalcogenides towards next-generation electronic devices: Recent advances and challenges, *Nanoscale Horiz.* **5**, 787 (2020).
- [13] Z. Zhang, Y. Gong, X. Zou, P. Liu, P. Yang, J. Shi, L. Zhao, Q. Zhang, L. Gu, and Y. Zhang, Epitaxial growth of two-dimensional metal–semiconductor transition-metal dichalcogenide vertical stacks ( $VSe_2/MX_2$ ) and their band alignments, *ACS Nano* **13**, 885 (2019).
- [14] J. Zhou, J. Qiao, C. G. Duan, A. Bourneil, K. L. Wang, and W. Zhao, Large tunneling magnetoresistance in  $VSe_2/MoS_2$  magnetic tunnel junction, *ACS Appl. Mater. Interfaces* **11**, 17647 (2019).
- [15] Z. I. Popov, N. S. Mikhaleva, M. A. Visotin, A. A. Kuzubov, S. Entani, H. Naramoto, S. Sakai, P. B. Sorokin, and P. V. Avramov, The electronic structure and spin states of 2D graphene/ $VX_2$  ( $X = S, Se$ ) heterostructures, *Phys. Chem. Chem. Phys.* **18**, 33047 (2016).
- [16] S. Manzeli, D. Ovchinnikov, D. Pasquier, O. V. Yazyev, and A. Kis, 2D transition metal dichalcogenides, *Nat. Rev. Mater.* **2**, 17033 (2017).
- [17] C. Battaglia, H. Cercellier, F. Clerc, L. Despont, M. G. Garnier, C. Koitzsch, P. Aebi, H. Berger, L. Forró, and C. Ambrosch-Draxl, Fermi-surface-induced lattice distortion in  $NbTe_2$ , *Phys. Rev. B* **72**, 195114 (2005).
- [18] H. W. Myron and A. J. Freeman, Electronic structure and Fermi-surface-related instabilities in  $1T-TaS_2$  and  $1T-TaSe_2$ , *Phys. Rev. B* **11**, 2735 (1975).
- [19] M. D. Johannes and I. I. Mazin, Fermi surface nesting and the origin of charge density waves in metals, *Phys. Rev. B* **77**, 165135 (2008).
- [20] F. Weber, S. Rosenkranz, J.-P. Castellán, R. Osborn, G. Karapetrov, R. Hott, R. Heid, K.-P. Bohnen, and A. Alatas, Electron-phonon coupling and the soft phonon mode in  $TiSe_2$ , *Phys. Rev. Lett.* **107**, 266401 (2011).
- [21] M. Calandra and F. Mauri, Charge-density wave and superconducting dome in  $TiSe_2$  from electron-phonon interaction, *Phys. Rev. Lett.* **106**, 196406 (2011).
- [22] K. Wijayarathne, J. Zhao, C. Malliakas, D. Y. Chung, M. G. Kanatzidis, and U. Chatterjee, Spectroscopic signature of moment-dependent electron–phonon coupling in  $2H-TaS_2$ , *J. Mater. Chem. C* **5**, 11310 (2017).
- [23] W. Kohn, Excitonic phases, *Phys. Rev. Lett.* **19**, 439 (1967).
- [24] A. Kogar, M. S. Rak, S. Vig, A. A. Husain, F. Flicker, Y. I. Joe, L. Venema, G. J. MacDougall, T. C. Chiang, E. Fradkin, and J. Van Wezel, Signatures of exciton condensation in a transition metal dichalcogenide, *Science* **358**, 1314 (2017).
- [25] E. Möhr-Vorobeva, S. L. Johnson, P. Beaud, U. Staub, R. De Souza, C. Milne, G. Ingold, J. Demsar, H. Schaefer, and A. Titov, Nonthermal melting of a charge density wave in  $TiSe_2$ , *Phys. Rev. Lett.* **107**, 036403 (2011).
- [26] J. Diego, D. Subires, A. H. Said, D. A. Chaney, A. Korshunov, G. Garbarino, F. Diekmann, S. K. Mahatha, V. Pardo, J. M. Wilkinson, and J. S. Lord, Electronic structure and lattice dynamics of  $1T-VSe_2$ : Origin of the three-dimensional charge density wave, *Phys. Rev. B* **109**, 035133 (2024).
- [27] T. Yilmaz, X. Tong, J. T. Sadowski, S. Hwang, K. Evans-Lutterodt, K. Kisslinger, and E. Vescovo, Evolution of the Fermi surface of  $1T-VSe_2$  across a structural phase transition, *Materials* **17**, 4498 (2024).
- [28] T. Yilmaz, X. Jiang, D. Lu, P. M. Sheverdyaeva, A. V. Matetskiy, P. Moras, F. Mazzola, I. Vobornik, J. Fujii, K. Evans-Lutterodt, and E. Vescovo, Dirac nodal arc in  $1T-VSe_2$ , *Commun. Mater.* **4**, 47 (2023).
- [29] J. Pandey and A. Soni, Electron-phonon interactions and two-phonon modes associated with charge density wave in single crystalline  $1T-VSe_2$ , *Phys. Rev. Res.* **2**, 033118 (2020).
- [30] J. Diego, A. H. Said, S. K. Mahatha, R. Bianco, L. Monacelli, M. Calandra, F. Mauri, K. Rossnagel, I. Errea, and S. Blanco-Canosa, van der Waals driven anharmonic melting of the 3D charge density wave in  $VSe_2$ , *Nat. Commun.* **12**, 598 (2021).
- [31] K. Rossnagel, On the origin of charge-density waves in select layered transition-metal dichalcogenides, *J. Phys.: Condens. Matter* **23**, 213001 (2011).
- [32] P. Monceau, Electronic crystals: An experimental overview, *Adv. Phys.* **61**, 325 (2012).
- [33] R. Hovden, A. W. Tsen, P. Liu, B. H. Savitzky, I. El Baggari, Y. Liu, W. Lu, Y. Sun, P. Kim, A. N. Pasupathy, and L. F. Kourkoutis, Atomic lattice disorder in charge-density-wave phases of exfoliated dichalcogenides ( $1T-TaS_2$ ), *Proc. Natl. Acad. Sci. USA* **113**, 11420 (2016).
- [34] S. Yoshizawa, K. Sagisaka, and H. Sakata, Visualization of alternating triangular domains of charge density waves in  $2H-NbSe_2$  by scanning tunneling microscopy, *Phys. Rev. Lett.* **132**, 056401 (2024).
- [35] A. Soumyanarayanan, M. M. Yee, Y. He, J. Van Wezel, D. J. Rahn, K. Rossnagel, E. W. Hudson, M. R. Norman, and J. E. Hoffman, Quantum phase transition from triangular to stripe charge order in  $NbSe_2$ , *Proc. Natl. Acad. Sci. USA* **110**, 1623 (2013).
- [36] Y. Nakata, K. Sugawara, A. Chainani, H. Oka, C. Bao, S. Zhou, P.-Y. Chuang, C.-M. Cheng, T. Kawakami, Y. Saruta, T. Fukumura, S. Zhou, T. Takahashi, and T. Sato, Robust charge-density wave strengthened by electron correlations in monolayer  $1T-TaSe_2$  and  $1T-NbSe_2$ , *Nat. Commun.* **12**, 5873 (2021).
- [37] M. Lee, M. Šiškins, S. Mañías-Valero, E. Coronado, P. G. Steeneken, and H. S. van der Zant, Study of charge density waves in suspended  $2H-TaS_2$  and  $2H-TaSe_2$  by nanomechanical resonance, *Appl. Phys. Lett.* **118**, 193105 (2021).
- [38] V. Petkov, K. Chapagain, S. Shastri, and Y. Ren, Genesis of the periodic lattice distortions in the charge density wave state of  $2H-TaSe_2$ , *Phys. Rev. B* **101**, 121114(R) (2020).
- [39] T. H. Choudhury, X. Zhang, Z. Y. Al Balushi, M. Chubarov, and J. M. Redwing, Epitaxial growth of two-dimensional layered transition metal dichalcogenides, *Annu. Rev. Mater. Res.* **50**, 155 (2020).

- [40] K. Tsutsumi, X-ray-diffraction study of the periodic lattice distortion associated with a charge-density wave in 1T-VSe<sub>2</sub>, *Phys. Rev. B* **26**, 5756 (1982).
- [41] J. A. Wilson, F. J. Di Salvo, and S. Mahajan, Charge-density waves and superlattices in the metallic layered transition metal dichalcogenides, *Adv. Phys.* **24**, 117 (1975).
- [42] J. van Landuyt, G. A. Wiegers, and S. Amelinckx, A new type of deformation modulated superstructure in 1T-VSe<sub>2</sub> and its relation with other superstructures in transition metal dichalcogenides, *Phys. Status Solidi A* **46**, 479 (1978).
- [43] K. K. Fung, J. W. Steeds, and J. A. Eades, Application of convergent beam electron diffraction to study the stacking of layers in transition-metal dichalcogenides, *Physica B+C (Amsterdam)* **99**, 47 (1980).
- [44] K. Terashima, T. Sato, H. Komatsu, T. Takahashi, N. Maeda, and K. Hayashi, Charge-density wave transition of 1T-VSe<sub>2</sub> studied by angle-resolved photoemission spectroscopy, *Phys. Rev. B* **68**, 155108 (2003).
- [45] T. Sato, K. Terashima, S. Souma, H. Matsui, T. Takahashi, H. Yang, S. Wang, H. Ding, N. Maeda, and K. Hayashi, Three-dimensional Fermi-surface nesting in 1T-VSe<sub>2</sub> studied by angle-resolved photoemission spectroscopy, *J. Phys. Soc. Jpn.* **73**, 3331 (2004).
- [46] J. Henke, F. Flicker, J. Laverock, and J. van Wezel, Charge order from structured coupling in VSe<sub>2</sub>, *SciPost Phys.* **9**, 056 (2020).
- [47] S. C. Bayliss and W. Y. Liang, Reflectivity and band structure of 1T-VSe<sub>2</sub>, *J. Phys. C: Solid State Phys.* **17**, 2193 (1984).
- [48] T. Yilmaz, E. Vescovo, and B. Sinkovic, Multiband Fermi surface in 1T-VSe<sub>2</sub> and its implication for the charge density wave phase, *Phys. Rev. B* **107**, 165109 (2023).
- [49] V. N. Strocov, M. Shi, M. Kobayashi, C. Monney, X. Wang, J. Krempasky, T. Schmitt, L. Patthey, H. Berger, and P. Blaha, Three-dimensional electron realm in VSe<sub>2</sub> by soft-x-ray photoelectron spectroscopy: Origin of charge-density waves, *Phys. Rev. Lett.* **109**, 086401 (2012).
- [50] Y. Falke, N. Ehlen, G. Marini, A. V. Fedorov, V. Y. Voroshnin, B. V. Senkovskiy, K. Nikonov, M. Hoesch, T. K. Kim, L. Petaccia, G. Di Santo, T. Szkopek, G. Profeta, and A. Grüneis, Coupling to zone-center optical phonons in VSe<sub>2</sub> enhanced by charge density waves, *Phys. Rev. B* **104**, 235137 (2021).
- [51] T. Yilmaz, E. Vescovo, J. T. Sadowski, and B. Sinkovic, Spectroscopic evidence of highly correlated electrons in VSe<sub>2</sub>, *Phys. Rev. B* **105**, 245114 (2022).
- [52] A. Wegner, D. Louca, and J. Yang, Local trigonal modes and the suppression of the charge density wave in TiSe<sub>2-x</sub>Te<sub>x</sub>, *Phys. Rev. B* **99**, 205110 (2019).
- [53] E. S. Bozin, M. Abeykoon, S. Conradson, G. Baldinozzi, P. Sutar, and D. Mihailovic, Crystallization of polarons through charge and spin ordering transitions in 1T-TaS<sub>2</sub>, *Nat. Commun.* **14**, 7055 (2023).
- [54] <https://2dsemiconductors.com/VSe2-Crystal>.
- [55] F. J. DiSalvo and J. V. Waszczak, Magnetic studies of VSe<sub>2</sub>, *Phys. Rev. B* **23**, 457 (1981).
- [56] H. P. Klug and L. E. Alexander, *X-Ray Diffraction Procedures for Polycrystalline and Amorphous Materials* (Wiley, New York, 1974).
- [57] P. Juhás, T. Davis, C. L. Farrow, and S. J. L. Billinge, PDFgetX3: A rapid and highly automatable program for processing powder diffraction data into total scattering pair distribution functions, *J. Appl. Crystallogr.* **46**, 560 (2013).
- [58] B. H. Toby and R. B. Von Dreele, GSAS-II: The genesis of a modern open-source all purpose crystallography software package, *J. Appl. Crystallogr.* **46**, 544 (2013).
- [59] Z. Wang, Q. Yin, S. Yan, L. Wu, X. Wu, M. Li, W. Song, Q. Liu, H. Ma, W. Ji, H. Lei, and S. Wang, Three-dimensional charge density wave observed by angle-resolved photoemission spectroscopy in 1T - VSe<sub>2</sub>, *Phys. Rev. B* **104**, 155134 (2021).
- [60] D. Wines, J. Tiihonen, K. Saritas, J. T. Krogel, and C. Ataca, A quantum Monte Carlo study of the structural, energetic, and magnetic properties of two-dimensional H and T phase VSe<sub>2</sub>, *J. Phys. Chem. Lett.* **14**, 3553 (2023).
- [61] See Supplemental Material at <http://link.aps.org/supplemental/10.1103/PhysRevB.111.014105> for results of DFT calculations and crystal structure modeling, which also contains Refs. [26,62–64].
- [62] J. P. Perdew, K. Burke, and M. Ernzerhof, Generalized gradient approximation made simple, *Phys. Rev. Lett.* **77**, 3865 (1996).
- [63] G. Kresse and J. Furthmüller, Efficient iterative schemes for *ab initio* total-energy calculations using a plane-wave basis set, *Phys. Rev. B* **54**, 11169 (1996).
- [64] A. Togo, F. Oba, and I. Tanaka, First-principles calculations of the ferroelastic transition between rutile-type and CaCl<sub>2</sub>-type SiO<sub>2</sub> at high pressures, *Phys. Rev. B* **78**, 134106 (2008); A. Togo and I. Tanaka, First principles phonon calculations in materials science, *Scr. Mater.* **108**, 1 (2015).
- [65] C. L. Farrow, P. Juhas, J. W. Liu, D. Bryndin, E. S. Bozin, J. Bloch, T. Proffen, and S. J. L. Billinge, PDFfit2 and PDFgui: Computer programs for studying nanostructure in crystals, *J. Phys.: Condens. Matter* **19**, 335219 (2007).
- [66] R. Amin, J. Pandey, K. Beyer, and V. Petkov, Two-step charge density wave transition and hidden transient phase in 1T-TiSe<sub>2</sub>, *Phys. Rev. B* **109**, 144106 (2024).
- [67] G. A. Wiegers, J. L. de Boer, A. Meetsma, and S. van Smaalen, Domain structure and refinement of the triclinic superstructure of 1T-TaSe<sub>2</sub> by single crystal x-ray diffraction, *Z. Kristallogr.* **216**, 45 (2001).
- [68] G. Duvjir, B. K. Choi, T. T. Ly, N. H. Lam, K. Jang, D. D. Dung, Y. J. Chang, and J. Kim, Multiple charge density wave phases of monolayer VSe<sub>2</sub> manifested by graphene substrates, *Nanotechnology* **32**, 364002 (2021).
- [69] P. Chen, Y.-H. Chan, R.-Y. Liu, H. T. Zhang, Q. Gao, A.-V. Fedorov, M. Y. Chou, and T.-C. Chiang, Dimensional crossover and symmetry transformation of charge density waves in VSe<sub>2</sub>, *Phys. Rev. B* **105**, L161404 (2022).
- [70] Á. Pásztor, A. Scarfato, C. Barreateau, E. Giannini, and C. Renner, Dimensional crossover of the charge density wave transition in thin exfoliated VSe<sub>2</sub>, *2D Mater.* **4**, 041005 (2017).
- [71] X. Shen, R. Heid, R. Hott, A. A. Haghighirad, B. Salzmann, M. dos Reis Cantarino, C. Monney, A. H. Said, M. Frachet, B. Murphy, K. Rossnagel, S. Rosenkranz, and F. Weber, Precursor region with full phonon softening above the charge-density-wave phase transition in 2H-TaSe<sub>2</sub>, *Nat. Commun.* **10**, 7282 (2023).
- [72] X. Xi, L. Zhao, Z. Wang, H. Berger, L. Forró, J. Shan, and K. F. Mak, Strongly enhanced charge-density-wave order in monolayer NbSe<sub>2</sub>, *Nat. Nanotechnol.* **10**, 765 (2015).
- [73] F. Weber, S. Rosenkranz, J.-P. Castellan, R. Osborn, R. Hott, R. Heid, K.-P. Bohnen, T. Egami, A. H. Said, and D. Reznik, Extended phonon collapse and the origin of the charge-density wave in 2H-NbSe<sub>2</sub>, *Phys. Rev. Lett.* **107**, 107403 (2011).